Journal of Materials Science & Technology 187 (2024) 188–194

Contents lists available at ScienceDirect

Journal of Materials Science & Technology

journal homepage: www.elsevier.com/locate/jmst

Letter

Atomic-scale structure and nonlinear optical absorption of two-dimensional GeS

1. Introduction

Layered van der Waals materials have emerged as a new class of materials with fascinating properties for versatile potential applications owing to their unique atomic structures and ultrathin thickness [1–7]. As a subcategory of layered van der Waals materials, group IV monochalcogenides, including Ge (S, Se, Te) and Sn (S, Se, Te), possess similar atomic structures and comparable electronic structures, rendering them becoming promising alternatives for applications in thermoelectric [8], ferroelectric [9–11], photocatalytic [12], optoelectronic [13–16], and memory devices [17–19]. Moreover, group IV monochalcogenides exhibit remarkable changes in electronic and optical responses by thinning layer numbers and tuning stacking sequences owing to their modified interlayer coupling and band structures, which enable the development of an ideal two-dimensional (2D) platform to fulfill novel optoelectronic devices.

Germanium sulfide (GeS), a representative group IV chalcogenide 2D material, has captured significant attention due to its emerging nanostructures, environmental compatibility, high electron mobility, and strong light-matter interaction. Its anisotropic structure and wide bandgap characteristics give rise to interesting electric, spintronic, and optical behaviors [20,21]. Furthermore, the electronic states of GeS are topography-, layer-, and defect-dependent, which triggers flexibility in structural design and performance manipulation, thereby providing a foundation for a broad range of applications [8,21,22]. Recently, layered GeS materials in different dimensions have been successfully synthesized, including 3D single crystals, 2D nanosheets and nanoribbons, and 1D helical nanowires. The corresponding energy bandgaps (E_g) undergo a substantial blue shift from 1.20–1.65 eV for a bulk crystal [23,24] to 0.76 eV [25] for a monolayer. The helical nanowires show a much larger bandgap of E_g (1.87–2.4) eV due to their radial size and screw angles [26]. Liu et al. reported that the electron conductivity and thermal conductivity of GeS nanowires are pivotal to thermoelectric applications and can be tailored by controlling the twisting morphology and defect engineering [8]. Additionally, GeS also exhibits intriguing optical properties. A 3D optical anisotropy due to the anisotropic crystal structure has been theoretically predicted and experimentally realized in ~100 nm-thick GeS nanosheets [14]. Sutter et al. revealed that GeS nanosheets terminated by edges or facets can serve as good alternatives for light emission, as the edges or facets can interfere with emitted light, resulting in the tuning of light emission by geometrical fashion [24]. Fan et al. have found that GeS nanosheets with a thickness of less than 5 nm exhibit enhanced light absorptions in the visible light and ultraviolet regions, and a layer-dependent photoresponsivity has been detected in the GeS-based photodetectors [13].

The crystal structure, thickness, and defect density of 2D materials often significantly affect their electronic, optical, mechanical, and thermal properties. For instance, the bandgap of a 2D material can be tuned by its thickness, and the electrical conductivity of a 2D material can be altered by introducing defects or controlling the orientation of its crystal structure [27,28]. Therefore, a fundamental understanding and manipulation of the microstructures of GeS are essential to identifying exceptional functional properties of ultrathin GeS materials, e.g., their optoelectronic performances.

Here, we conduct a systematical three-dimensional analysis of the atomic-scale structure of GeS van der Waals materials and investigate their nonlinear optical properties. We find that the GeS nanosheets show exceptional nonlinear optical properties with an effective nonlinear coefficient (β_{eff}) of -0.318 cm/GW and a nonlinear refractive index coefficient (n_2) of 0.52×10^{-18} m^2/W, making them a highly promising nonlinear optical media for ultrafast laser generation. Noticeably, the Tm-doped fiber laser upon the GeS nanosheets produces robust and stable ultrashort pulses at the center wavelength of 1934 nm. These findings indicate the potential of GeS for integrated nonlinear photonic applications in the mid-infrared waveband.

2. Experimental

GeS single crystals with an orthorhombic structure were prepared via chemical vapor transport (CVT) using I_2 powder as a transport additive (Fig. S1(a) in Supplementary Information). GeS single crystals were then thinned into layered flakes/nanosheets via the tape-assisted mechanical and liquid-phase exfoliation methods (Fig. S1(b)). Raman spectra were measured using a Confocal Raman Microscope (WITec Alpha300M+, Witec Ulm Germany) with an excitation wavelength of 532 nm at 0.5 mW for 10 s with a 1800 g/mm grating. The X-ray photoelectron spectroscope (XPS) data were collected using an ESCALABE 250Xi spectrometer (Thermo Scientific) with monochromatic Al $K\alpha$ X-rays. The scanning probe microscopy (AFM) images were acquired in a tapping mode using a AFM microscope (AFM Dimension Icon, Bruker) at ambient atmosphere. The energy-dispersive X-ray spectroscopy (EDX) analysis was performed in a probe-corrected FEI Titan G2 ChemiSTEM operated at an accelerating voltage of 200 kV. The atomic-resolution high-angle annular dark-field scanning transmission electron microscopy (HAADF STEM) and bright-field STEM (BF STEM) imaging were carried out using a double Cs-corrected Titan G3 Cubed Themis operated at 200 kV. The high-resolution TEM (HRTEM) images and selected-area electron diffraction (SAED) patterns were taken on a JEOL JEM-2100 TEM operated at 200 kV. The nonlinear absorption characteristics were investigated by the open aperture (OA) and closed aperture (CA) Z-scan methods

https://doi.org/10.1016/j.jmst.2023.10.056

[29]. A mode-locked ultrafast pulse was generated at 2 μm by integrating GeS nanosheets saturable absorber (SA) with thulium (Tm)-doped fiber laser. A detailed description of the experimental section is given in the Supplementary Information.

3. Result and discussion

3.1. Synthesis, structure, and morphology

Fig. S2 shows the EDS mapping of a GeS flake prepared by mechanical exfoliation, indicating that the GeS crystal is well formed with a homogeneous distribution of Ge and S elements. A quantitative chemical analysis reveals a 1:1 atomic ratio of Ge:S in the flake. The microstructure of the flake was systematically investigated by high-resolution STEM imaging (Fig. 1) and electron diffraction simulation (Fig. S3). The atomic-column imagings of GeS flakes were taken along the [001], [011], [101], and [012] zone axes, as illustrated by their corresponding structural models in Fig. 1(a–d). The STEM images and the fast Fourier transform (FFT) patterns (Fig. 1(e–h)) confirm that the GeS flakes have an orthorhombic crystalline structure in the space group Pnma [21]. Further analysis of the STEM images reveals a high degree of crystallographic perfection for the GeS crystal. Note that the STEM images were collected from different TEM samples, and no visible structural distortions or extra super-lattice diffraction spots can be detected compared to the simulated diffraction patterns in Fig. S3. We also present the zoom-in HAADF STEM images (Fig. 1(i–l)) and BF STEM images (Fig. 1(m–p)) viewed along the [001], [011], [101], and [012] directions, where the atomic columns with periodically strong and weak intensity can be identified because the brightness of the HAADF signal increases with the averaged atomic number (Z) as $\sim Z^{1.7}$ [30,31]. This dependence makes the HAADF signal from heavy atoms much brighter than that from light ones, which gives the inverse contrast for each column in a BF-STEM image. Thus, individual Ge and S atoms can be clearly distinguished from the enlarged HAADF STEM images, in which bright spots represent Ge atoms and dark spots S atoms. We also conducted an annular bright-field (ABF) image simulation, which further confirms the crystal structure of GeS (Fig. 1(q–t)).

Since mechanical exfoliation falls short of scalability, i.e., it is rather hard to produce large quantities of few-layered 2D materials [32], we also adopted liquid-phase exfoliation, which is emerging as a promising approach for large-scale production of 2D materials. The NMP solvent was chosen for the exfoliation of GeS due to its low intralayer to interlayer force constants ratio and low chemical stability in ambient conditions [33]. The size and thickness of the liquid-phase exfoliated GeS nanosheets are greatly affected by the centrifugation velocity. The main size of the GeS nanosheets

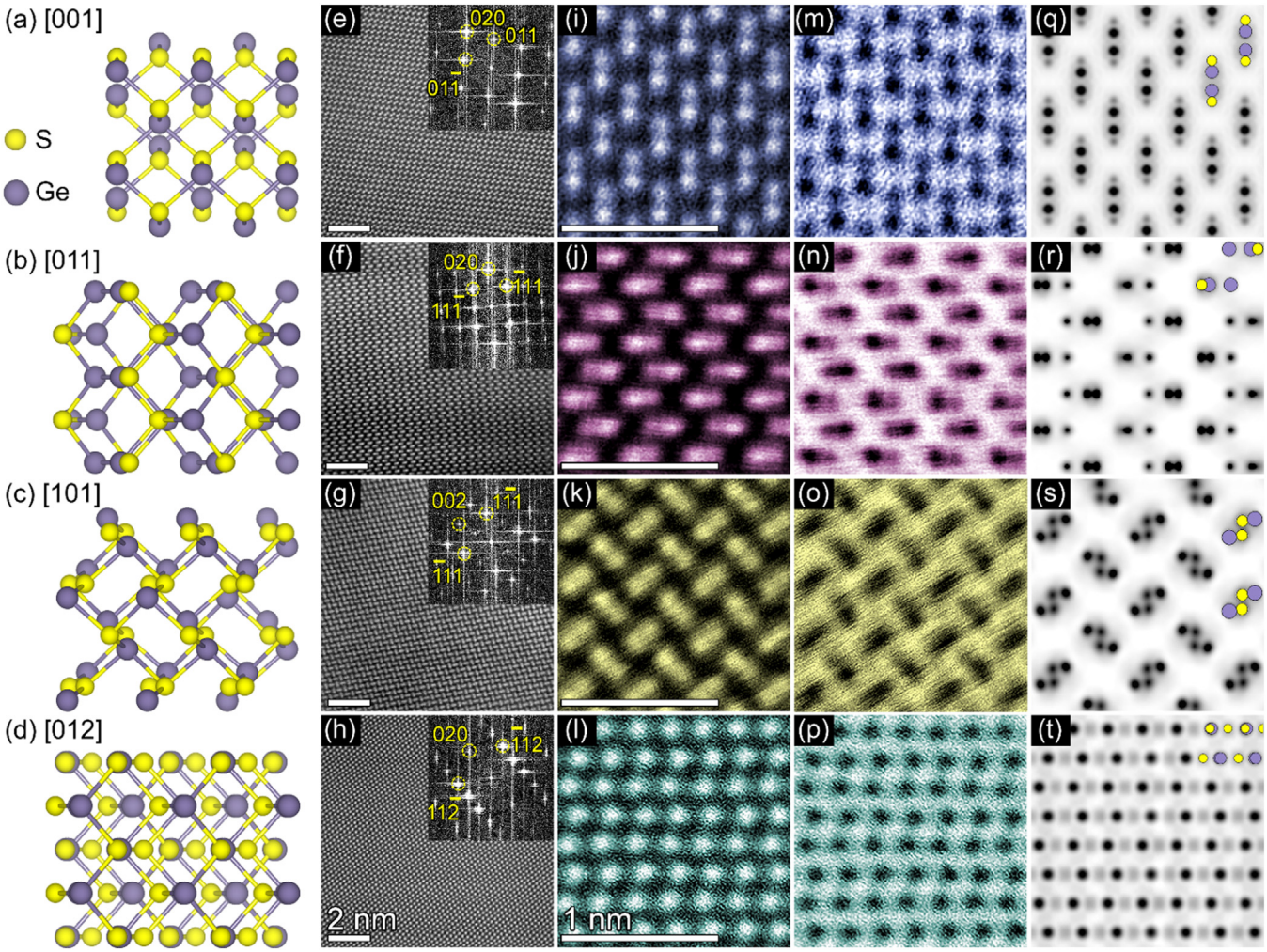

Fig. 1. Microstructural characterization of GeS. (a–d) Atomic models of the GeS lattice viewed along [001], [011], [101], and [012] zone axis. (e–h) HAADF STEM images taken along different directions. The inset shows the corresponding fast-Fourier transform patterns. (i–l) Enlarged HAADF STEM images. (m-p) Enlarged BF STEM images. (q–t) Simulated ABF STEM images.

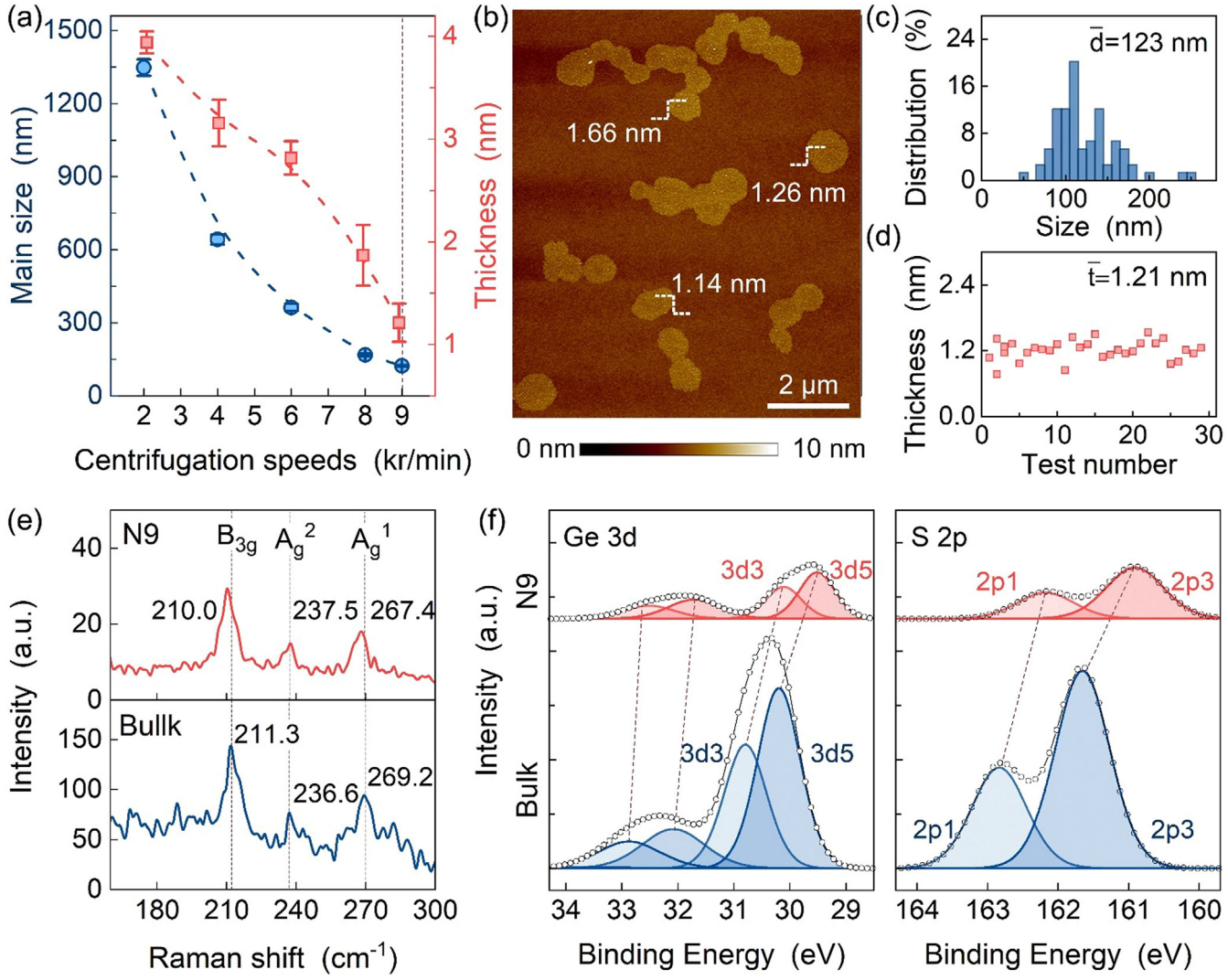

Fig. 2. (a) Size and thickness of GeS nanosheets with a centrifugation velocity from 2000 r/min to 9000 r/min. (b) AFM image, (c) size distribution, and (d) thickness of the prepared GeS nanosheets. (e) Raman spectra and (f) high-resolution XPS spectra from the Ge 3d and S 2p regions for the GeS nanosheets and bulk GeS.

decreases from 1348 ± 335 nm to 123 ± 37 nm, and their average thickness reduces from 3.94 ± 0.41 nm to 1.21 ± 0.19 nm when the centrifugation velocity increases from 2000 r/min to 9000 r/min (Fig. 2(a)). Given the fine lateral dimension and atomic thickness, the GeS nanosheets centrifuged at 9000 r/min (N9-GeS) are selected for subsequent experiments. The AFM imaging clearly shows that the GeS spin-coated on a SiO_2/Si substrate is well separated with a lateral dimension ranging from 50 nm to 250 nm and an average topographic height of 0.77–1.538 nm, which corresponds to 2, 3 atomic layers of GeS (Fig. 2(b–d)).

Raman and XPS characterization of the GeS were further carried out together with those of bulk GeS as a reference (Fig. 2(e, f)). As shown in Fig. 2(e), three Raman peaks at 211.3, 236.6, and 269.2 cm^{-1} are visible, which correspond to the in-plane B_{3g}, A_g^2, and A_g^1 shear vibration modes, respectively, as can be confirmed in the bulk GeS [13]. Similar Raman frequencies are observed for the GeS, indicating that the atomically thin GeS maintains structural integrity after exfoliation. Notably, the GeS sample shows a shift in Raman peak shifts and a decrease in peak intensity, which may be attributed to the thickness effect and interference effect that cause variation in the in-plane atomic vibration (B_{3g} and A_g) [34]. The XPS peaks at ~162.8 and ~161.6 eV are assigned to the S $2p_{1/2}$ and S $2p_{3/2}$ of the Ge-S bonds, respectively [35]. After the liquid exfoliation, the S $2p_{1/2}$ and S $2p_{3/2}$ peaks exhibit an apparent right-shift of 0.65 and 0.75 eV, respectively. Similarly, the XPS peaks of the Ge $3d_{3/2}$ and Ge $3d_{5/2}$ of the Ge-S bonds also shift notably to the lower binding energy compared to those of the ultrathin nanosheets achieved from bulk GeS via the liquid-exfoliation method. The shift in the XPS peak generally reflects changes in the electron transfer and electronic configuration between the nearest-neighbor atoms [36–38]. Therefore, the noticeable right-shift of the S 2p and Ge 3d peaks confirms that the bonding environment and electron density distribution of the S and Ge elements somewhat alter due to the liquid exfoliation, consistent with the Raman results.

Fig. 3(a) shows the ADF and the corresponding EDS elemental mapping, revealing that Ge and S elements are uniformly distributed in the whole nanosheets, which confirms the formation of pure atomic-layer GeS nanosheets. The HRTEM images of the GeS sample collected along [001] and [010] directions (Fig. 3(c, d)) show that the GeS nanosheets maintain their bulk structure (Fig. S4). However, compared to the HRTEM images in Fig. S4, one can note additional structural distortion in the GeS nanosheet, indicating that the periodic layered structure is somewhat destroyed after chemical exfoliation. The change in crystallography is also confirmed by the corresponding fast Fourier transform

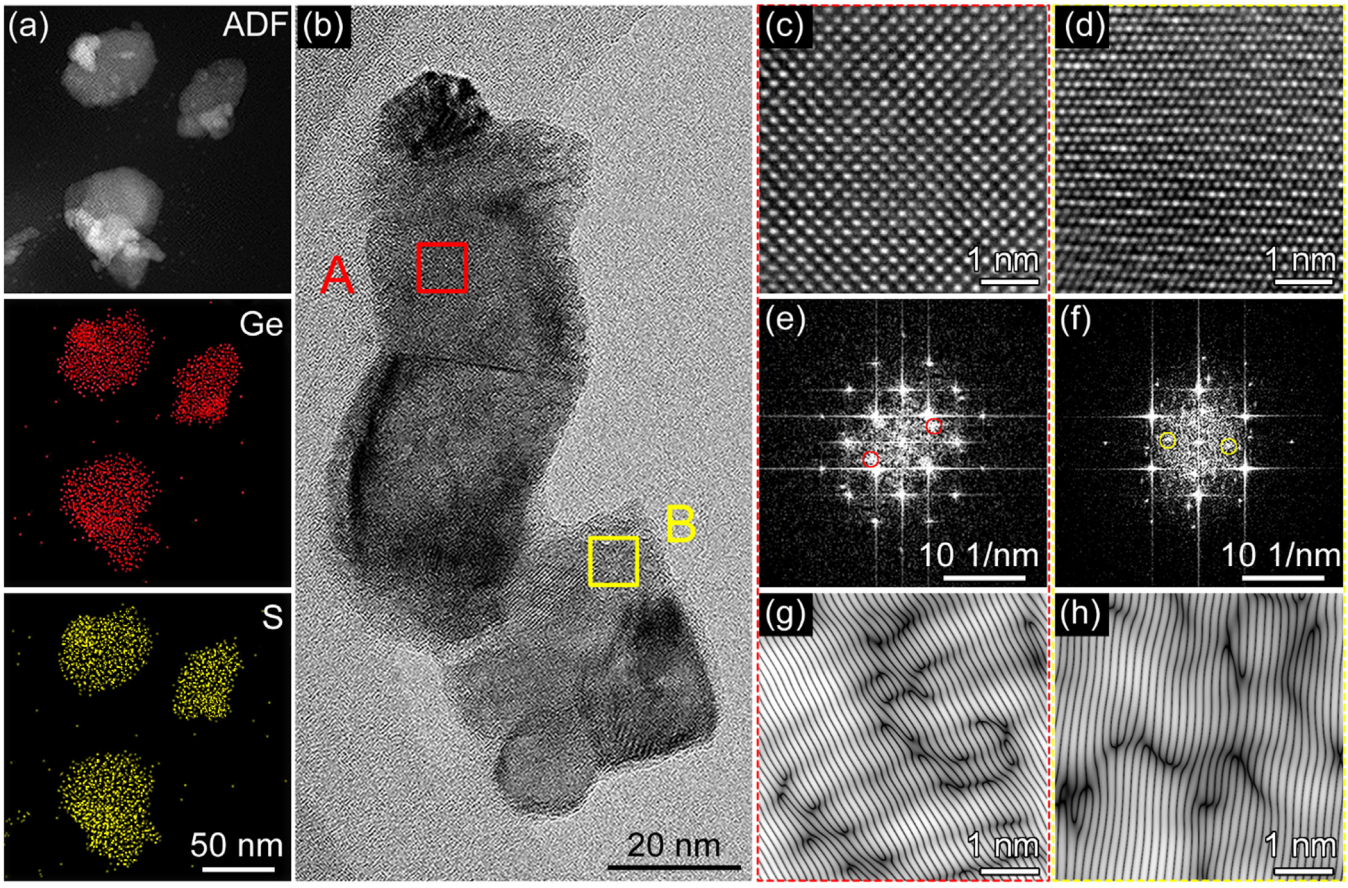

Fig. 3. Chemical composition and microstructure analysis of the GeS nanosheet. (a) ADF STEM image and the corresponding EDS mappings for the Ge and S elements. (b) TEM image with two regions (A) and (B) highlighted. (c, d) HRTEM images taken from (c) region A and (d) region B in (b). (e–h) (e, f) Corresponding FFT patterns and (g, h) IFFT images for the region A (e, g) and B (f, h).

(FFT) patterns (Fig. 3(e, f)) and inverse fast Fourier transform (IFFT) patterns (Fig. 3(g, h)). The extra diffraction spots in FFT patterns (indicated by circles) and lattice distortions in the IFFT images confirm the degradation in the crystallinity of the GeS nanosheet.

3.2. Optical nonlinearity characteristics

The optical nonlinearity characteristics of GeS are related to its atomic structure and thickness. The band gap of a bulk GeS is 1.6 eV, whereas the band gap of ultrathin GeS nanosheets (less than 5 layers) ranges from 1.69 eV to 1.9 eV [13,14]. The structural distortion in the GeS nanosheets could generate shear forces between layers and provide additional electronic states, leading to exciting optical responses [39]. Using the reliable Z-scan measurement method, the effective nonlinear absorption coefficient (β_{eff}) and the nonlinear refractive index coefficient (n_2) could be determined, e.g., the nonlinear optical response of the GeS nanosheets could be investigated [40]. The schematic setup used in the study can be found in Ref. [41]. Figs. 4(a) and S5 show the open aperture (OA) and closed aperture (CA) Z-scan profiles for the GeS nanosheet measured with an excitation wavelength centered at 1800 nm. The noise of optical response may be attributed to the degraded crystallinity of the GeS nanosheets, including recoverable deformation and surface damage [39]. An evident saturable absorption phenomenon is identified as the normalized transmission increases nonlinearly with decreasing distance between the sample and the focus point ($Z = 0$) (Fig. 4(a)).

By fitting the experimental data of the OA Z-scan configurations, the largest value of β_{eff} is determined to be -0.318 cm/GW. Such a negative β_{eff} value further confirms the saturable absorption. Note that the β_{eff} value of the GeS nanosheet is comparable to the previously reported data for 2D materials and is about 10^3 times larger in magnitude than those of the BPQDs/PMMA composite nanofiber films [42]. The typical peak-valley type signal of the CA Z-scan profile (Fig. S5) indicates a self-focusing nonlinear optical response with a positive n_2 value of 0.52×10^{-18} m^2/W [43]. Fig. 4(b) illustrates the nonlinear saturable absorption property of the GeS sample measured via a power-dependent method at 1800 nm. The saturable absorption feature is quite evident when the peak power intensity increases. Based on Fig. 4(b) and the equation $T = 1\text{-}\ [\alpha_s/(1+I/I_s)]\text{-}\alpha_{ns}$, the modulation depth ($\alpha_s$), saturation intensity (I_s), and unsaturable loss (α_{ns}), which are known as the three primary parameters in assessing the saturable absorption performance, are estimated to be 41.35 %, 53.1 GW/cm^2, and 39.92 %, respectively (Table S1 in Supplementary Information). The findings suggest that 2D GeS holds potential applications as an optical modulator for generating ultrafast pulses in the mid-infrared wavelength region, offering a feasible solution to the lack of efficient optical modulators [44].

A saturable absorber (SA) fabricated using the GeS was integrated into a Tm-doped passively mode-locked fiber laser to achieve mode-locking at 1934 nm (Fig. S6). Fig. 4(c–f) shows the characteristics of the mode-locked pulses obtained by regulating the PC at a pump power of 840 mW. The optical spectrum of the mode-locked pulses is centered at 1933.96 nm with a 3-dB

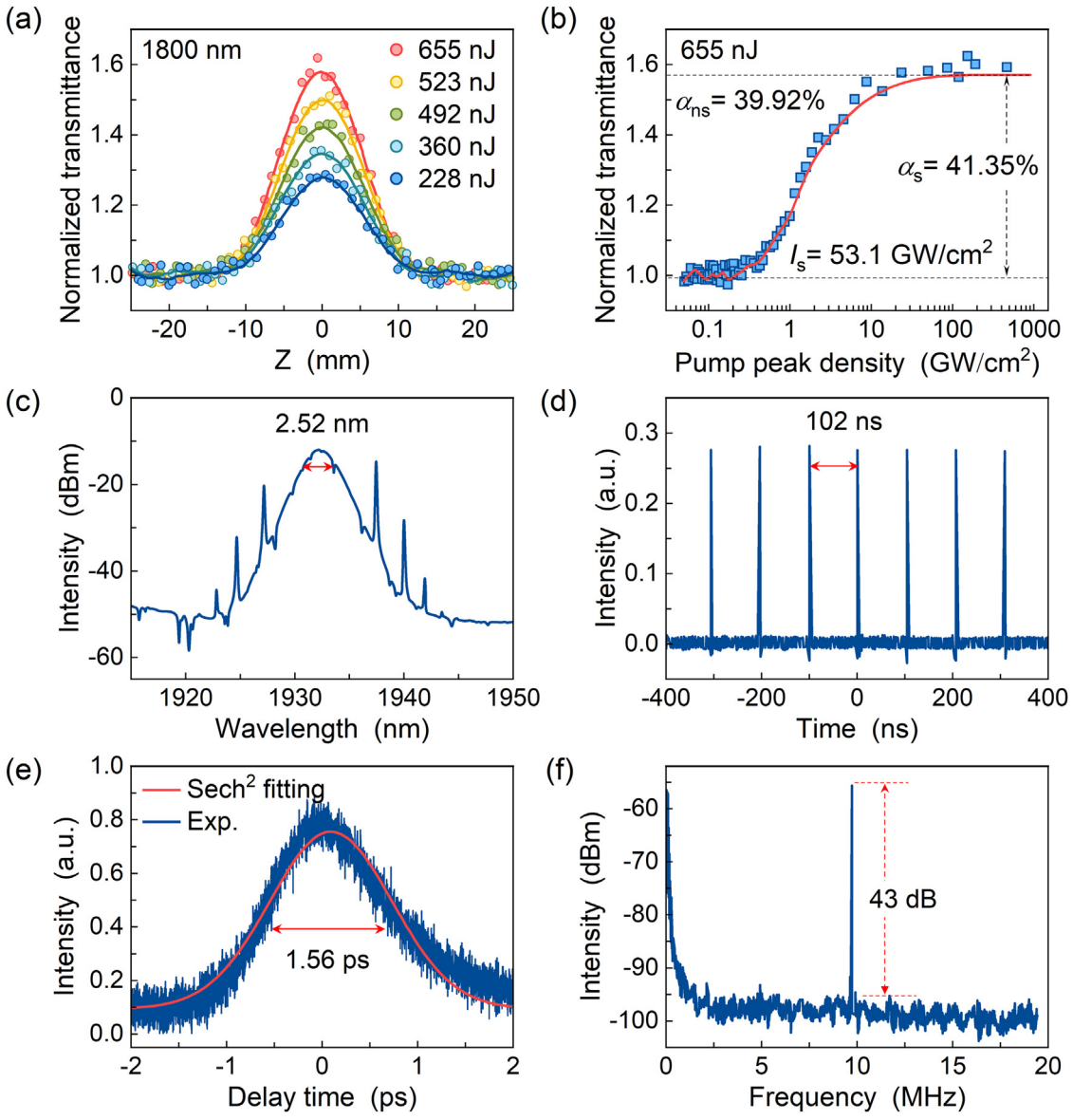

Fig. 4. Optical measurements of the GeS nanosheets. Nonlinear optical characterization of the GeS sample recorded at 1800 nm: (a) open-aperture (OA) Z-scan traces and (b) relationship between the normalized transmittance and input peak intensity. (c–f) Ultrafast pulse generation near 2 μm using the GeS nanosheets as a saturable absorber. (c) Output mode-locked pulse spectrum with a spectral bandwidth of 2.52 nm at 3 dB. (d) Mode-locking pulse train with ~102 ns interval. (e) Autocorrelation trace with a pulse duration of ~1.56 ps fitted by a Sech^2 function. (f) Radiofrequency (RF) spectrum with a single-to-noise ratio of 43 dB at ~9.7 MHz. The solid lines represent theoretical fitting to the experimental data.

bandwidth of 2.52 nm (Fig. 4(c)). The stable symmetrical Kelly sidebands in the output spectrum indicate a soliton mode-locked laser [45]. The output pulse train in Fig. 4(d) has a pulse train interval of approximately 102 ns (i.e., repetition rate of 9.7 MHz), which verifies the mode-locking state of the laser. Fig. 4(e) plots the experimental intensity autocorrelation trace fitted with a sech^2 profile, from which the pulse full width at half maximum is calculated to be 1.56 ps, leading to a time-bandwidth product (TBP) of 0.317. The TPB value of the GeS-based laser is very close to the Fourier transform limit of 0.315, which is deemed the smallest pulse duration for a given spectral width [46]. The radio frequency (RF) spectrum of the mode-locked pulse has a signal-to-noise ratio of 43 dB (>10^4 contrast) at the cavity fundamental repetition rate of 9.7 MHz (Fig. 4(f)). Further analysis of the wideband RF spectrum confirms that the GeS laser enables the generation of high-stabile mode-locking pulses (Fig. S7). These results demonstrate that the GeS nanosheets are an excellent candidate for ultrafast laser pulse generation devices.

4. Conclusion

We have comprehensively characterized the atomic-scale structure and chemical composition of GeS nanosheets from various zone axes and investigated their optical properties. The GeS nanosheets with an average thickness of 1.21 ± 0.19 nm can be fulfilled by the liquid-phase exfoliation, which induces structural distortions. We demonstrate that the GeS nanosheets could yield a significant effective nonlinear coefficient of -0.318 cm/GW, holding potential for ultrafast photonics application in the mid-infrared range. We further employ the GeS nanosheets to fabricate saturable absorbers for a Tm-doped mode-locked fiber laser and show that a highly stable and ultrafast pulse of 1.56 ps can be generated at near 2 μm wavelength. These findings offer critical

insights into the unique 2D structures of GeS for emerging ultrafast photonics applications, opening up an avenue in manipulating the ultrafast pulse generation capability of 2D material-based saturable absorbers by defect engineering.

Declaration of competing interest

The authors declare that they have no known competing financial interests or personal relationships that could have appeared to influence the work reported in this paper.

Acknowledgments

This work was financially supported by the China Postdoctoral Science Foundation (Nos. 2020M673174 and 2019M663688). The authors acknowledge the European Research Executive Agency (Project No. 101079184-FUNLAYERS).

Supplementary materials

Supplementary material associated with this article can be found, in the online version, at doi:10.1016/j.jmst.2023.10.056.

References

[1] W. Li, X. Qian, J. Li, Nat. Rev. Mater. 6 (2021) 829–846.
[2] Q. Qiu, Z. Huang, Adv. Mater. 33 (2021) 2008126.
[3] J. Kim, Y. Lee, M. Kang, L. Hu, S. Zhao, J.H. Ahn, Adv. Mater. 33 (2021) 2005858.
[4] F. He, Y. Zhou, Z. Ye, S.H. Cho, J. Jeong, X. Meng, Y. Wang, ACS Nano 15 (2021) 5944–5958.
[5] Y. Zhang, S. Li, Z. Li, H. Liu, X. Liu, J. Chen, X. Fang, Nano Lett. 21 (2021) 382–388.
[6] Y. Zhang, J. Yao, Z. Zhang, R. Zhang, L. Li, Y. Teng, Z. Shen, L. Kang, L. Wu, X. Fang, J. Mater. Sci. Technol. 164 (2023) 95–101.
[7] Y. Zhang, J. Yao, Y. Teng, Z. Zhang, L. Wang, X. Wang, Y. Li, L. Kang, J.H. He, X. Fang, Nano Energy 117 (2023) 108915.
[8] Y. Liu, J. Wang, S. Kim, H. Sun, F. Yang, Z. Fang, N. Tamura, R. Zhang, X. Song, J. Wen, B.Z. Xu, M. Wang, S. Lin, Q. Yu, K.B. Tom, Y. Deng, J. Turner, E. Chan, D. Jin, R.O. Ritchie, A.M. Minor, D.C. Chrzan, M.C. Scott, J. Yao, Nature 570 (2019) 358–362.
[9] H. Yin, C. Liu, G.P. Zheng, Y. Wang, F. Ren, Appl. Phys. Lett. 114 (2019) 192903.
[10] Y. Zhu, X. Wang, W. Mi, J. Mater. Chem. C 7 (2019) 2049–2058.
[11] S. Song, Y. Zhang, J. Guan, S. Dong, Phys. Rev. B 103 (2021) L140104.
[12] D. Gu, X. Tao, H. Chen, W. Zhu, Y. Ouyang, Q. Peng, Nanoscale 11 (2019) 2335–2342.
[13] X. Fan, L. Su, F. Zhang, D. Huang, D.K. Sang, Y. Chen, Y. Li, F. Liu, J. Li, H. Zhang, H. Xie, ACS Appl. Mater. Interfaces 11 (2019) 47197–47206.
[14] Z. Li, Y. Yang, X. Wang, W. Shi, D.J. Xue, J.S. Hu, ACS Appl. Mater. Interfaces 11 (2019) 24247–24253.
[15] Q. Wu, Z. Fang, Y. Zhu, H. Song, Y. Liu, X. Su, D. Pan, Y. Gao, P. Wang, S. Yan, Z. Fei, J. Yao, Y. Shi, Nano Lett. 22 (2022) 5086–5093.
[16] I.B. Kherchachi, A. Attaf, H. Saidi, A. Bouhdjer, H. Bendjedidi, Y. Benkhetta, R. Azizi, J. Semicond. 37 (2016) 032001.
[17] S. Jia, H. Li, T. Gotoh, C. Longeaud, B. Zhang, J. Lyu, S. Lv, M. Zhu, Z. Song, Q. Liu, J. Robertson, M. Liu, Nat. Commun. 11 (2020) 4636.
[18] A. Ali, H. Abbas, M. Hussain, S.H.A. Jaffery, S. Hussain, C. Choi, J. Jung, Appl. Mater. Today 29 (2022) 101554.
[19] S. Zhang, B. Song, S. Jia, R. Cao, S. Liu, H. Xu, Q. Li, J. Semicond. 43 (2022) 104101.
[20] M. Feng, S.C. Liu, L. Hu, J. Wu, X. Liu, D.J. Xue, J.S. Hu, L.J. Wan, J. Am. Chem. Soc. 143 (2021) 9664–9671.
[21] E. Sutter, B. Zhang, M. Sun, P. Sutter, ACS Nano 13 (2019) 9352–9362.
[22] E. Sutter, J.S. French, H.P. Komsa, P. Sutter, ACS Nano 16 (2022) 3735–3743.
[23] M. Rakshit, S. Nath, S. Chowdhury, R. Mondal, D. Banerjee, D. Jana, Phys. Scr. 97 (2022) 125804.
[24] P. Sutter, C. Argyropoulos, E. Sutter, Nano Lett. 18 (2018) 4576–4583.
[25] B. Ul Haq, S. AlFaify, A. Laref, R. Ahmed, F.K. Butt, A.R. Chaudhry, S.U. Rehman, Q. Mahmood, Ceram. Int. 45 (2019) 18073–18078.
[26] E. Sutter, P. Sutter, Small 17 (2021) 2104784.
[27] Y. Cao, V. Fatemi, S. Fang, K. Watanabe, T. Taniguchi, E. Kaxiras, P. Jarillo-Herrero, Nature 556 (2018) 43–50.
[28] J. Zhang, R. Sun, D. Ruan, M. Zhang, Y. Li, K. Zhang, F. Cheng, Z. Wang, Z.M. Wang, J. Appl. Phys. 128 (2020) 100902.
[29] X. Jiang, S. Liu, W. Liang, S. Luo, Z. He, Y. Ge, H. Wang, R. Cao, F. Zhang, Q. Wen, J. Li, Q. Bao, D. Fan, H. Zhang, Laser Photonics Rev. 12 (2018) 1700229.
[30] D.A. Muller, Nat. Mater. 8 (2009) 263–270.
[31] Z. Wang, M. Saito, K.P. McKenna, L. Gu, S. Tsukimoto, A.L. Shluger, Y. Ikuhara, Nature 479 (2011) 380–383.
[32] Z. Guo, H. Zhang, S. Lu, Z. Wang, S. Tang, J. Shao, Z. Sun, H. Xie, H. Wang, X.F. Yu, P.K. Chu, Adv. Funct. Mater. 25 (2015) 6996–7002.
[33] D. Lam, K.S. Chen, J. Kang, X. Liu, M.C. Hersam, Chem. Mater. 30 (2018) 2245–2250.
[34] S. Lee, K. Kim, K.P. Dhakal, H. Kim, W.S. Yun, J. Lee, H. Cheong, J.H. Ahn, Nano Lett. 17 (2017) 7744–7750.
[35] Y. Wei, J. He, Q. Zhang, C. Liu, A. Wang, H. Li, T. Zhai, Mater. Chem. Front. 1 (2017) 1607–1614.
[36] Y. Sun, K. Xu, Z. Wei, H. Li, T. Zhang, X. Li, W. Cai, J. Ma, H.J. Fan, Y. Li, Adv. Mater. 30 (2018) 1802121.
[37] Z. Li, L. Wang, R. Liu, Y. Fan, H. Meng, Z. Shao, G. Cui, S. Pang, Adv. Energy Mater. 9 (2019) 1902142.
[38] Y. Sun, X. Li, T. Zhang, K. Xu, Y. Yang, G. Chen, C. Li, Y. Xie, Angew. Chem. Int. Ed. 60 (2021) 21575–21582.
[39] C. Zhang, K.V. Larionov, K.L. Firestein, J.F.S. Fernando, C.E. Lewis, P.B. Sorokin, D.V. Golberg, Nano Lett. 22 (2022) 673–679.
[40] M. Sheik-Bahae, A.A. Said, T. Wei, D.J. Hagan, E.W.V. Stryland, IEEE J. Quantum Electron. 26 (1990) 760–769.
[41] H. Zhang, S.B. Lu, J. Zheng, J. Du, S.C. Wen, D.Y. Tang, K.P. Loh, Opt. Express 22 (2014) 7249–7260.
[42] Y. Xu, W. Wang, Y. Ge, H. Guo, X. Zhang, S. Chen, Y. Deng, Z. Lu, H. Zhang, Adv. Funct. Mater. 27 (2017) 1702437.
[43] I. Abdelwahab, P. Dichtl, G. Grinblat, K. Leng, X. Chi, I.H. Park, M.P. Nielsen, R.F. Oulton, K.P. Loh, S.A. Maier, Adv. Mater. 31 (2019) 1902685.
[44] H. Chen, F. Wang, M. Liu, M. Qian, X. Men, C. Yao, L. Xi, W. Qin, G. Qin, C. Wu, Laser Photonics Rev 13 (2019) 1800326.
[45] Q. Bao, H. Zhang, Y. Wang, Z. Ni, Y. Yan, Z.X. Shen, K.P. Loh, D.Y. Tang, Adv. Funct. Mater. 19 (2009) 3077–3083.
[46] F. Wang, A.G. Rozhin, V. Scardaci, Z. Sun, F. Hennrich, I.H. White, W.I. Milne, A.C. Ferrari, Nat. Nanotechnol. 3 (2008) 738–742.

Jijun Zhang[1]
Guangdong Engineering and Technology Research Centre for Advanced Nanomaterials, School of Environment and Civil Engineering, Dongguan University of Technology, Dongguan 523808, China
International Iberian Nanotechnology Laboratory (INL), Avenida Mestre José Veiga, Braga 4715-330, Portugal
Institute of Fundamental and Frontier Sciences, University of Electronic Science and Technology of China, Chengdu 610054, China

Rong Sun[1]
International Iberian Nanotechnology Laboratory (INL), Avenida Mestre José Veiga, Braga 4715-330, Portugal

Yanqi Ge[1]
Guangdong Engineering and Technology Research Centre for Advanced Nanomaterials, School of Environment and Civil Engineering, Dongguan University of Technology, Dongguan 523808, China

Jingyi Wang, Zexuan Wang
International Iberian Nanotechnology Laboratory (INL), Avenida Mestre José Veiga, Braga 4715-330, Portugal

Lijian Meng
CIETI, ISEP, Polytechnic of Porto, Rua Dr. António Bernardino de Almeida, Porto 4249-015, Portugal

Francis Leonard Deepak
International Iberian Nanotechnology Laboratory (INL), Avenida Mestre José Veiga, Braga 4715-330, Portugal

Min Zhang
Guangdong Engineering and Technology Research Centre for Advanced Nanomaterials, School of Environment and Civil Engineering, Dongguan University of Technology, Dongguan 523808, China

Peng Yin
School of Information and Communication, National University of Defence Technology, Wuhan 430035, China

Faliang Cheng*
Guangdong Engineering and Technology Research Centre for Advanced Nanomaterials, School of Environment and Civil Engineering, Dongguan University of Technology, Dongguan 523808, China

Zhiming Wang*
Institute of Fundamental and Frontier Sciences, University of Electronic Science and Technology of China, Chengdu 610054, China

Zhongchang Wang*
International Iberian Nanotechnology Laboratory (INL), Avenida Mestre José Veiga, Braga 4715-330, Portugal

*Corresponding authors.
E-mail addresses: chengfl@dgut.edu.cn (F. Cheng), zhmwang@uestc.edu.cn (Z. Wang), zhongchang.wang@inl.int (Z. Wang)

[1] These authors contributed equally to this work.

Revised 25 October 2023